JOURNAL OF Applied Polymer SCIENCE

Modification of Epoxy-Anhydride Thermosets with a Hyperbranched Poly(ester amide). II. Thermal, Dynamic Mechanical, and Dielectric Properties and Thermal Reworkability

Xavier Fernández-Francos,[1] Andrzej Rybak,[2] Robert Sekula,[2] Xavier Ramis,[3] Francesc Ferrando,[4] Lidia Okrasa,[5] Angels Serra[1]

[1]Department of Analytical and Organic Chemistry, Universitat Rovira i Virgili, C/Marcel·lí Domingo s/n, Tarragona 43007, Spain
[2]ABB Corporate Research Center, Starowislna 13A, 31-038 Krakow, Poland
[3]Thermodynamics Laboratory, Escola Tècnica Superior d'Enginyeria Industrial de Barcelona (ETSEIB), Universitat Politècnica de Catalunya, Av. Diagonal 647, 08028, Barcelona, Spain
[4]Department of Mechanical Engineering, University Rovira i Virgili, C/Països Catalans 26, 43007 Tarragona, Spain
[5]Department of Molecular Physics, Technical University of Lodz, Zeromskiego 116, Lodz 90-924, Poland
Correspondence to: X. Fernández-Francos (E-mail: xavier.fernandez@urv.cat)

ABSTRACT: An epoxy–anhydride formulation used for the coating electrical devices was modified with a commercially available hyperbranched poly(ester amide), Hybrane S2200, to improve the thermal degradability of the resulting thermoset and, thus, facilitate the recovery of substrate materials after the service life of the component. The thermomechanical, mechanical, and dielectric properties and thermal degradability were studied and interpreted in terms of the composition and network structure of the cured thermosets. Although the crosslinking density was significantly reduced with the incorporation of S2200, the glass transition temperature of the fully cured material ($T_{g\infty}$) of the modified thermoset was hardly affected because of the enhancement of H-bonding interactions in the presence of S2200. Despite the different network structures, the combined dielectric and dynamic mechanical analysis revealed that the relaxation dynamics of both networks were very similar. In terms of application, improvements in the dielectric and mechanical properties were observed. The incorporation of S2200 accelerated the thermal decomposition of the material and, thus, facilitated the recovery of the valuable parts from the substrate at the end of the service life of the apparatus. © 2012 Wiley Periodicals, Inc. J. Appl. Polym. Sci. 128: 4001–4013, 2013

KEYWORDS: degradation; dendrimers; dielectric properties; hyperbranched polymers and macrocycles; thermal properties; thermosets

Received 11 June 2012; accepted 1 August 2012; published online 17 October 2012
DOI: 10.1002/app.38453

INTRODUCTION

Epoxy resins are widely used in a variety of applications because of their good thermomechanical, adhesive, and electrical properties; thermal and chemical stability; and ease of processing. However, their high thermal stability, caused by the densely crosslinked network achieved in the curing process and the nature of the covalent linkages of the network structure, can be a drawback in what is called *reworkability*. Reworkability can be achieved by the introduction of thermally cleavable linkages in the network structure. A controlled thermal degradation can lead to a partial breakdown of the network structure of the material; this reduces its mechanical properties and facilitates its removal by mechanical means. This can be interesting in certain applications, such as microelectronics, where the replacement of a faulty chip can be accomplished without the whole assembly or the electrical components, of which the metallic substrate can be recovered after the life cycle of the component is expired, wasting away. In the early work of Chen and coworkers,[1–3] they reported the use of a newly synthesized epoxy monomer with cleavable tertiary ester groups that could be used as modifiers in epoxy formulations. However, the use of cycloaliphatic monomers restricts their application and curing versatility. Some of us have reported the modification of epoxy formulations with a variety of lactones[4–6] or cyclic carbonates;[7] this results in the incorporation of ester or carbonate groups into the network structure and, thus, enhances the thermal degradability of the resulting materials. The main drawback in this case is the reduction of the glass transition temperature of the fully cured material ($T_{g\infty}$) via the decrease in the crosslinking density and the flexibility of the units introduced into the network structure.

Hyperbranched polymers (HBPs) are a type of dendronized polymers, which can be used as effective polymer modifiers of

© 2012 Wiley Periodicals, Inc.

thermosetting materials because of (1) their high degree of branching, which makes them less viscous than their linear counterparts with the same equivalent molecular weight and (2) the high concentration of surface groups, which can be modified to fine-tune their physical compatibility with the matrix or make possible their covalent linkage to the matrix. The properties of the final material can thus be tailored as a function of the core structure, the degree of branching, and the type of functional end groups.[8] One of the most relevant applications in thermosets is their use as toughening agents that phase-separate during curing[9–15] or else get incorporated into the network structure.[16] Recently, we studied the use of hyperbranched poly(ester amide)s as modifiers for epoxy–anhydride formulations.[17] The presence of terminal OH groups in HBP facilitated its incorporation into the network structure. There was a significant lowering of the thermal stability of the resulting materials because of the presence of ester groups in the HBP structure, although their thermomechanical behavior was not compromised. Indeed, the impact strength (IS) of the resulting materials could even be improved.[17] In contrast, the use of a hyperbranched polyester did not improve the thermal degradability of thermosets,[18] but they were, nevertheless, chemically reworkable by hydrolysis of the ester groups in HBP. In this study, we aimed to profit from the enhanced thermal degradability of hyperbranched poly(ester amide)s with a view toward obtaining thermosets for electrical applications with comparable $T_{g\infty}$ values and mechanical and electrical properties with respect to those of the unmodified one, but which could facilitate the recovery of the substrate by controlled thermal degradation. Reactive HBPs with ester groups in their structure and hydroxyl groups as chain ends appeared to be good candidates for this purpose because (1) the covalent bonding of the multifunctional reactive HBP into the network structure could ensure that the thermomechanical behavior of the material was not compromised and (2) the presence of ester groups in HBP facilitated the thermal degradability of the resulting network structure of the thermoset.

To the best of our knowledge, the use of reactive HBPs as polymeric modifiers with the purpose of improving the reworkability of the modified thermosets is a novel approach that has not been explored in depth. Moreover, in this study, this strategy is offered as a specific solution for meeting the demands of an industrial partner. For this to be implemented as a real industrial application, one must bear in mind that enhanced reworkability should not be attained at the expense of other properties. Within this framework, relevant properties, such as the thermal conductivity and dielectric behavior, which were not determined in previous studies,[17] need to also be considered. The thermal and mechanical properties are also of key importance for application.[19] Further knowledge can be derived from the relationship between the effect of the modifier on these selected properties with the network structure of the thermoset and its chemical composition and, eventually, the curing kinetics. Such a relationship needs to be well understood for future material design.

In a previous article, we reported the curing kinetics of an unmodified and modified formulation with a hydroxyl-terminated hyperbranched poly(ester amide), Hybrane S2200.[20] The objective of this study was to examine in detail the effect of S2200 on the structure and properties of the modified formulation in comparison with the unmodified material and to explore its potential reworkability. The thermomechanical properties were determined with differential scanning calorimetry (DSC), dynamic mechanical analysis (DMA), and thermomechanical analysis (TMA). The thermal stability was studied with thermogravimetric analysis (TGA). Dielectric analysis (DEA) and thermal conductivity measurements were performed to assess the performance of the newly obtained materials for the selected application. Impact tests were performed to analyze the effect of the modifier on the fracture toughness of the resulting thermoset and the microhardness, which is a valuable parameter in the evaluation of coatings.

EXPERIMENTAL

Materials and Sample Preparation

Diglycidyl ether of bisphenol A (DGEBA; Araldite CY 228-1, Huntsman Advanced Materials (Europe) BVBA, Everberg, Belgium, 390–410 g/mol) and methyltetrahydrophtalic anhydride (MTHPA; Aradur HY 918, Huntsman, 166 g/mol) were used as received. Benzyldimethylamine (DY 062, Huntsman) was used as an initiator. A hyperbranched polyesteramide (S2200, Hybrane S2200, DSM, Zwolle, The Netherlands, obtained from succinic anhydride and diisopropanolamine building blocks, 175.9 g/equiv of OH) was used as received. Scheme 1 shows the structure of all of the starting products.

The DGEBA–MTHPA formulation (DG) were prepared by the addition of appropriate amounts of each reactant and initiator to a vial with mechanical stirring. For the preparation of the formulation with S2200 (DGS2200), appropriate amounts of DGEBA and S2200 were heated up to 150°C with a thermal gun, and the mixture was homogenized with mechanical stirring. After the mixture was cooled, anhydride was added, and the resulting mixture was homogenized with mechanical stirring. A corresponding amount of initiator was added to the vial and mixed with a mechanical stirrer. For both formulations, the amount of initiator was 1 phr with respect to the anhydride. Table I reports the compositions of the DG and DGS2200 formulations. As in previous studies,[17,20,21] an overstoichiometric amount of anhydride with respect to the epoxy was used in the DGS2200 formulation.

For the analysis of the material properties, samples of both formulations were cured at 100°C for 5 h and then postcured at 180°C for 2 h. The samples for DMA, TMA, and mechanical tests were cured in open Teflon molds. A silicone mold was used for the preparation of samples for DEA and thermal conductivity. The open surfaces of the samples were polished. The samples for TGA were cured in closed 0.5 mm thick Teflon molds. All of the samples were wrapped in Parafilm and stored in sealed plastic bags to prevent water absorption before use.

Characterization Techniques

DSC. A Mettler (Schwerzenbach, Switzerland) DSC822e calorimeter was used to determine the $T_{g\infty}$ values of the materials cured after the previous procedure, as the halfway point in the heat capacity step with the Richardson method of STARe software. Three experiments were performed for each formulation, and the results were averaged.

Fourier Transform Infrared (FTIR) Spectroscopy. A Bruker (Ettlingen, Germany) Vertex 70 FTIR spectrometer equipped

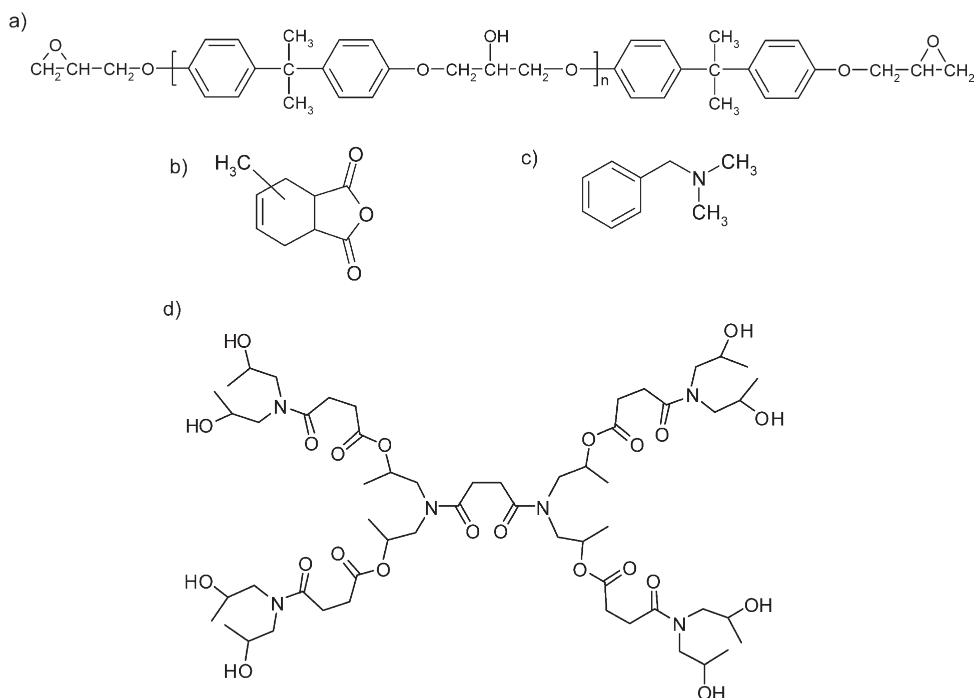

Scheme 1. Schemes of (a) DGEBA, (b) MTHPA, (c) benzyldimethylamine, and (d) idealized structure of S2200.

with an attenuated total reflectance device with temperature control (Golden Gate heated single-reflection diamond attenuated total reflectance Specac-Teknokroma) was used to obtain the FTIR spectra of the cured materials. The FTIR spectrometer was used at a resolution of 4 cm^{-1}, and 20 scans were averaged for each spectrum. To correct the penetration depth of the radiation in the samples, the spectra were multiplied by $W/1000$, where W is the wave number. A background was run before every series of measurements.

TMA. A Mettler (Schwerzenbach, Switzerland) TMA 40 thermomechanical analyzer was used to determine the thermal expansion coefficients of the samples cured after the previous curing schedule below and above their $T_{g\infty}$ value. Samples about 5 mm in diameter and 1.5 mm thick were sandwiched between two silica discs and heated at 5°C/min from 30 to 150°C in the first scan and up to 180°C in the second scan, which was used for the calculations. A blank curve determined with only the silica discs was subtracted. The expansion curves of three samples were averaged. The coefficients of thermal expansion (α_g and α_l) below and above $T_{g\infty}$, respectively, were calculated as follows:

$$\alpha = \frac{1}{L_0} \cdot \frac{dL}{dT} = \text{constant} \tag{1}$$

where L and L_0 are the thicknesses at any temperature and at room temperature, respectively.

Table I. Composition of the Formulations Studied

Formulation	MTHPA (wt %)	S2200 (wt %)	DGEBA/ MTHPA mass ratio	Epoxy/OH/ anhydride molar ratio
DG	45.98	0	1:0.851	1:0.106:1.025
DGS2200	42.91	15	1:1.019	1:0.48:1.2

The number of hydroxyl groups was calculated with the assumption of molecular masses of 390 g/mol for DGEBA and 175.9 g/equiv of OH for S2200.

DMA. A TA Instruments (New Castle, DE) DMA Q800 was used in single-cantilever mode with prismatic rectangular samples with dimensions of about 10 × 12 × 1.5 mm^3. The samples were heated at 3°C/min from 30 to 180°C at 1 Hz with an oscillation amplitude of 20 μm. Two scans were performed on each sample to check the reproducibility, and the results were averaged. Time–temperature superposition (TTS) experiments were performed by isothermal frequency sweeps (20, 10, 5, 2, 1, 0.5, 0.2, and 0.1 Hz) every 5°C from 80 to 180°C after 5 min of temperature equilibration at every step. Rheology Advantage software by TA Instruments (New Castle, DE) was used to perform the TTS adjustment of the experimental data.

DEA. The dielectric measurements were carried out with a Novocontrol system (Hundsangen, Germany) composed of an Alpha frequency response analyzer and a Quattro temperature controller. The samples were prepared in the form of sheets with thicknesses of 1.0–1.2 mm with gold electrodes evaporated *in vacuo*. The samples were sandwiched between two copper electrodes 20 mm in diameter and placed inside a temperature-controlled sample cell. The complex permittivity [$\varepsilon^*(f) = \varepsilon'(f) + i\varepsilon''(f)$, where ε' and ε'' are the real and the imaginary part of the complex permittivity ε^*, respectively] was determined in the frequency (f) range from 10^{-1} to 5×10^5 Hz and in the temperature range from −80 to 160°C. The alternating-current voltage applied to the capacitor was equal to 1.0 V. The

temperature was controlled with a nitrogen gas cryostat, and the temperature stability of the sample was better than 0.2°C. The points used for the activation maps, that is, the relaxation times (τs) at a given temperature (T), were determined by WinFIT (Hundsangen, Germany) software using the Havriliak–Negami function fitting.

TGA. A Mettler (Schwerzenbach, Switzerland) TGA 50 was used to study the thermal degradation of the materials. Samples weighing approximately 10 mg and 0.5 mm thick were heated at 10°C/min from 40 to 700°C in a nitrogen atmosphere. A blank curve was run and subtracted from the experiments. Three samples were analyzed for each formulation, and the results were averaged. The isothermal degradation of the materials was studied. The samples were preheated at 100°C/min and kept at 300, 350, and 400°C for up to 4 h (e.g., the 400°C samples were degraded only for 2 h). A blank curve was subtracted for each sample. The samples were then removed and, when possible, were analyzed with FTIR spectroscopy, and the glass-transition temperature (T_g) was determined with DSC.

Thermal Conductivity. Cylindrical specimens, with a diameter of 6 mm and a height of 3 mm, were cut for thermal measurements. Thermal conductivity measurements were performed by means of a physical property measurement system with a thermal transport option made by Quantum Design, Inc. (San Diego, CA). The sample was mounted in the two-probe-lead configuration, that is, spliced to the copper leads by the epoxy bound. Heat was applied by a current running through the copper lead. The thermal conductivity measurements were performed under high-vacuum conditions and at room temperature. To check the reliability of the measurements for each type of composite, two samples with different thicknesses were investigated. Additionally, on each sample, at least 10 measurements after the applied heat pulses were made to check the reproducibility of the results.

Mechanical Tests. Impact tests were performed at room temperature by means of an Izod 5110 impact tester according to ASTM D 4508-05 with rectangular samples ($25 \times 12 \times 2.5$ mm^3). The pendulum we used had a kinetic energy of 1 J. For each material, nine determinations were made. The IS was calculated from the energy absorbed by the sample upon fracture as follows:

$$IS = \frac{E - E_0}{S} \quad (2)$$

where E and E_0 are the energy loss of the pendulum with and without sample, respectively, and S is the cross section of the samples.

Microhardness was measured with a Wilson Wolpert (Micro Knoop 401 MAV) device according to ASTM D 1474-98. For each material, 10 determinations were made with a confidence level of 95%. The Knoop microhardness (HKN) was calculated from the following equation:

$$HKN = L/A_p = L/l^2 \cdot C_p \quad (3)$$

where L is the load applied to the indenter (0.025 kg), A_p is the projected area of indentation (mm^2), l is the measured length of the long diagonal of indentation in mm, and C_p is the indenter constant (7.028×10^{-2}) relating l^2 to A_p.

Density Measurements. The density of the cured formulations (ρ_{T0}) at room temperature was determined indirectly as the density of a KBr solution with a density equal to the sample and measured with a pycnometer. Two measurements were made for each sample, which corresponded to a solution density slightly higher or lower than that of the sample. Three samples were analyzed for each formulation, and the results were averaged.

Theoretical

According to the rubber elasticity theory,[22] the relaxed modulus (E'_r) can be related to the concentration of elastically active network chains υ_e (mol/kg) in the following manner:

$$E'_r = \phi \cdot 3 \cdot R \cdot T \cdot \upsilon_e \cdot \rho_T \quad (4)$$

where R is the gas constant, T is the absolute temperature at the measurement, usually 50°C above $T_{g\infty}$, ρ_T is the density of the material, and ϕ is a factor reflecting all of the nonidealities and deviations from the ideal behavior.

ρ_T of a given thermoset at any temperature T above $T_{g\infty}$ can be calculated with the density of the cured samples measured at room temperature (ρ_{T0}) and the linear thermal expansion data obtained by TMA as follows:

$$\rho_T = \frac{\rho_{T0}}{1 + 3 \cdot \alpha_g \cdot (T_g - T_0) + 3 \cdot \alpha_1 \cdot (T - T_g)} \quad (5)$$

where α_g and α_l are the linear thermal expansion coefficients below and above $T_{g\infty}$, respectively, and ρ_{T0} is the density of the cured thermoset at room temperature.

The TTS principle can be applied to the DEA and DMA data to analyze the main relaxation phenomena. For the main relaxation (α relaxation), the experimental data can be fitted to the Williams–Landel–Ferry (WLF) expression:[22,23]

$$\log \alpha_T = \frac{-C_1 \cdot (T - T_{ref})}{C_2 + T - T_{ref}} \quad (6)$$

where the shift factors (a_T's) can be calculated as $a_T = \nu_{ref}/\nu$, where ν_{ref} and ν correspond to the frequency at the reference temperature (T_{ref}) and the frequency at any other temperature, respectively. Equivalently, if τ is known, the a_T values can be calculated as $a_T = \tau/\tau_{ref}$, where τ_{ref} is the relaxation time at T_{ref}.

From the C_1 and C_2 parameters, the apparent activation energy (E_A) of the structural relaxation can be calculated[23] as follows:

$$E_A = \frac{\ln 10}{1000} \cdot R \cdot C_1 \cdot T_{ref}^2/C_2 \quad (7)$$

If one assumes that the relaxation of the network is governed by the evolution of free volume,[23] the fraction of free volume (f_g) at the relaxation can be calculated with the following expression:

$$f_g = \frac{1}{\ln 10 \cdot C_1} \quad (8)$$

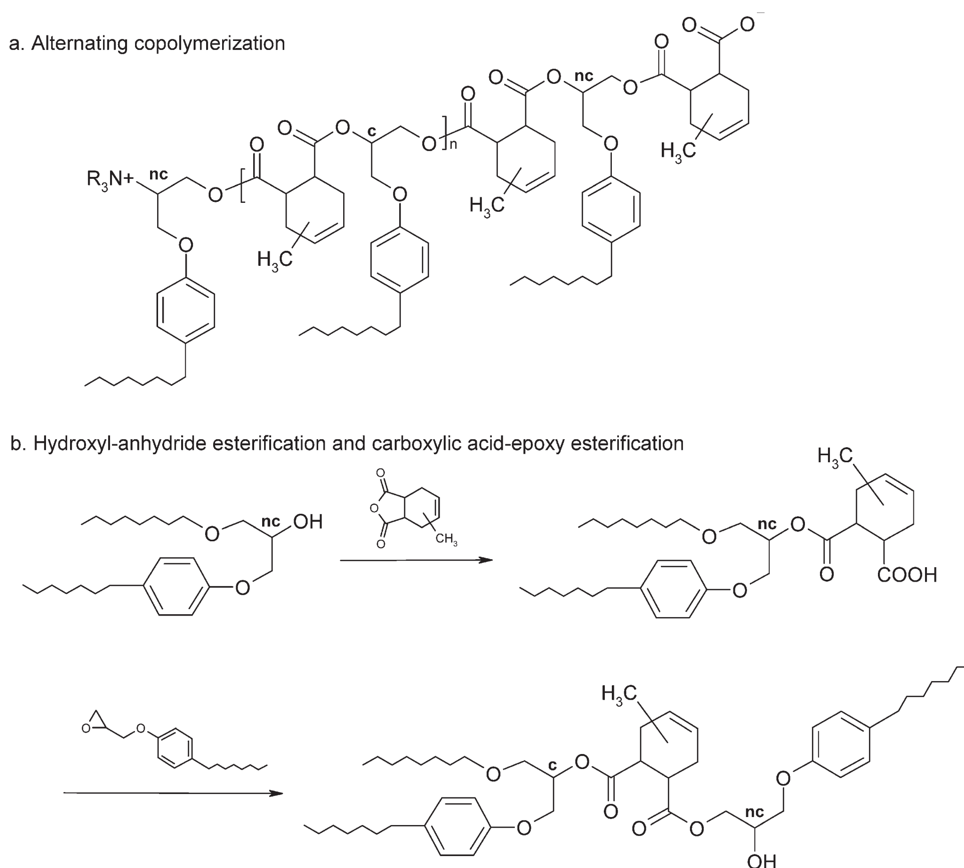

Scheme 2. Summary of the most significant reaction pathways in the curing of the epoxy–anhydride thermosets. Potential crosslinking points are noted with c, whereas noncrosslinking points are noted with nc.

It is also well known that the temperature dependence of secondary relaxations follows an Arrhenius law and, therefore, E_A can be determined as follows:

$$-\ln\tau = \ln A - \frac{E_A}{R\cdot T} \quad (9)$$

where τ is the relaxation time at a given temperature T and A is the pre-exponential factor.

RESULTS

Before we go on to analyze the material properties, we briefly discuss the curing mechanism as determined in our previous study.[20] The curing mechanism of epoxy–anhydride formulations, summarized in Scheme 2, is quite complex. To begin with, the presence of a tertiary amine promotes the anionic alternating copolymerization of epoxy and anhydride groups [Scheme 2(a)], but the presence of hydroxyl groups favors the uncatalyzed hydroxyl–anhydride copolymerization [Scheme 2(b)] and leads to the formation of carboxylic acid. The subsequent esterification of epoxy groups with carboxylic acid can take place with the aid of a tertiary amine.[24] It must also be pointed out that whereas the anionic copolymerization [Scheme 2(a)] is a ring-opening polyaddition process, the other esterification reactions follow polycondensation reaction kinetics. The presence of S2200 accelerated the reaction of both anhydride and epoxy groups because of the presence of hydroxyl groups, which could react with anhydride groups but could also accelerate the initiation with the tertiary amine. The regeneration of the tertiary amine, as reported in other studies,[25,26] could also take place. Homopolymerization of the epoxy groups was observed to occur to a very limited extend. The reaction of S2200 was gradual, and its incorporation into the network structure could be assured by the early carboxylic acid formation, subsequent reaction with epoxy groups (Scheme 3), and the occurrence of chain-transfer reactions.

Thermal and Dynamic Mechanical Properties

The results of the DSC analysis of both formulations are summarized in Table II. We observed that the incorporation of 15% S2200 decreased the $T_{g\infty}$ about 9°C as measured by DSC. This decrease in $T_{g\infty}$ could have been related to an increase in the mobility of the network structure caused by the incorporation of S2200. This was also accompanied by an increase in the change in C_p (ΔC_p), as commonly observed for thermosets,[22] which pointed to a loosening of the network structure due to the incorporation of S2200.

DMA of the DG and DGS2200 formulations is shown in Table II and Figure 1, which shows the α relaxation related to the glass transition of the thermoset. In agreement with the calorimetric data, a discrete decrease in $T_{g\infty}$ was observed, by a drop in the storage modulus (E'), tan δ peak temperature, or loss

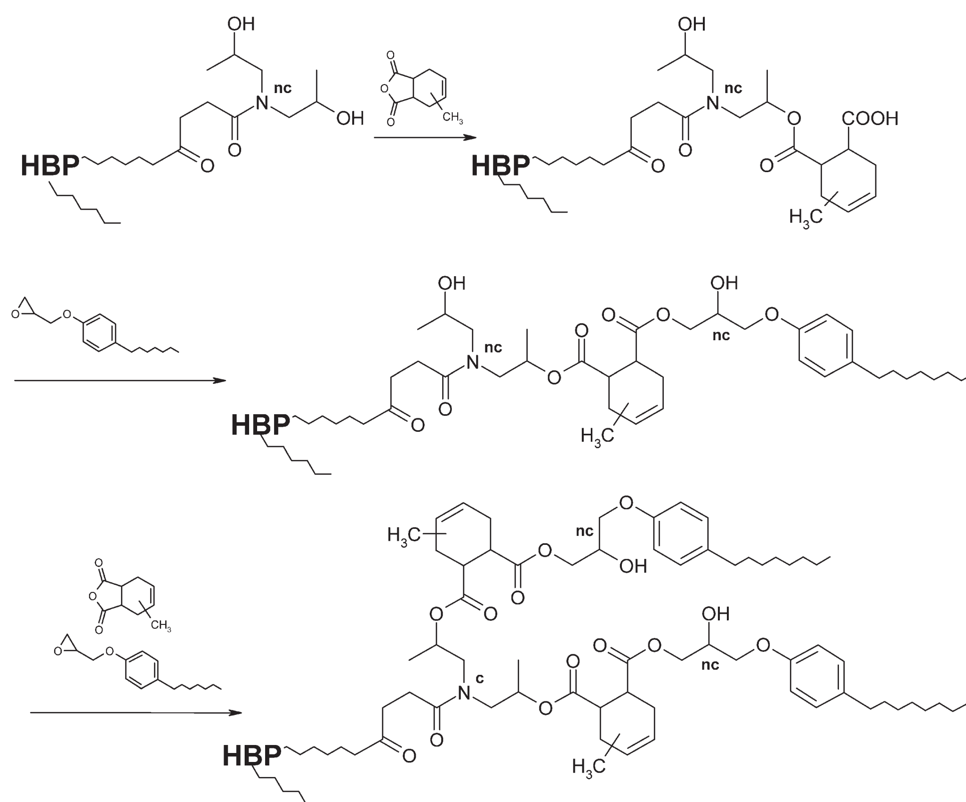

Scheme 3. Reaction pathway of S2200 hydroxyl groups. Potential crosslinking points are noted with c, whereas noncrosslinking points are noted with nc.

modulus peak temperature. We observed that the relaxations of the DG and DGS2200 formulations were unimodal; that is, in both cases we had homogeneous network structures, but some differences must be pointed out. First, the broader relaxation peak of DGS2200 [tan δ, full width at half-maximum (FWHM) in Table II] indicated that the DGS200 network was more disperse. Second, the energy dissipated during the relaxation,

Table II. Summary of the Dynamic Mechanical Properties Determined by DSC and DMA

	DG	DGS2200
DSC		
$T_{g\infty}$ (°C)	109.2 ± 4.3	101.3 ± 0.3
ΔC_p (J g^{-1} K^{-1})	0.299 ± 0.009	0.328 ± 0.008
DMA		
E' at 40°C (MPa)	2772 ± 82	2736 ± 80
E'_r (tan δ peak, T + 50°C; MPa)	17.70 ± 0.28	9.65 ± 0.04
Tan δ peak T (°C)	122.0 ± 0.7	114.4 ± 0.1
Tan δ peak height	1.06 ± 0.02	1.18 ± 0.01
Tan δ FWHM (°C)	15.0 ± 0.1	17.6 ± 0.2
Tan δ area (°C)	15.9 ± 0.3	20.8 ± 0.3
E'' peak T (°C)	112.6 ± 1.6	104.2 ± 0.1
E'' peak (MPa)	322 ± 6	375 ± 9

The results are reported as Value ± Error.

which was equivalent to the area below the tan δ peak (tan δ area in Table II) was higher for the DGS2200 formulation; this indicated that the material had better damping capabilities. Third, E'_r (E' measured 50°C above the relaxation) was reduced significantly in the DGS2200 formulation; this, according to eq. (4), was indicative of a lower υ_e. On the other hand, although the values may have been affected by the clamping and geometry, we observed that the unrelaxed E' (measured at the start of heating at 40°C) was a good order of magnitude compared with the Young's modulus values of epoxy thermosets[22] and that it was virtually unaffected by the incorporation of S2200.

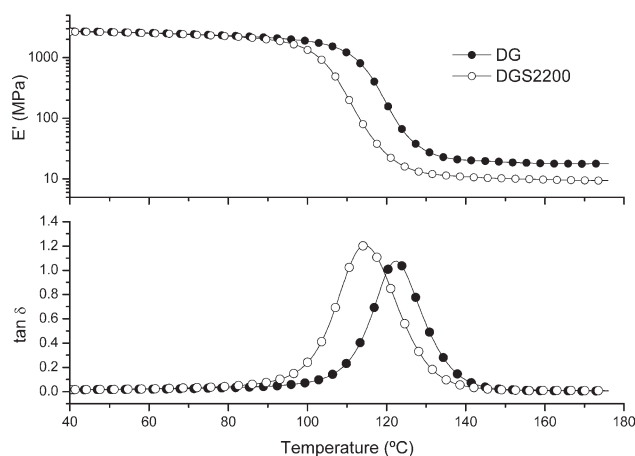

Figure 1. E' and tan δ curves with respect to temperature at 1 Hz.

To understand the thermal and dynamic mechanical properties of the DG and DGS2200 thermosets, one must consider the network structure resulting from the incorporation of S2200 into an epoxy–anhydride thermoset and relate this to the curing kinetics. The epoxy–anhydride network consists, basically, of an alternating copolymer sequence where the DGEBA epoxy groups turn to crosslinking units according to the anionic alternating mechanism depicted in Scheme 2(a). However, we found that the hydroxyl–anhydride esterification [Scheme 2(b)] and the subsequent carboxylic acid–epoxy esterification played an important part because of the increase in hydroxyl groups by tertiary amine regeneration and the presence of S2200. Moreover, because of the early exhaustion of anhydride groups during curing of the DG formulation, epoxy polyetherification could occur to some extent.[20]

We estimated the theoretical degree of crosslinking in the fully cured networks of DG and DGS2200. To do so, we made the following assumptions:

1. Overall, in the anionic copolymerization and the epoxy homopolymerization, the ring opening of a DGEBA epoxy group leads to a crosslinking point, given that there are two epoxy groups in DGEBA.
2. Upon initiation, there is a chain start and a chain end, which decrease the amount of crosslinks to twice the amount of initiating species. This is illustrated in Scheme 2(a), where it is shown that only the middle epoxy groups may issue three chains with infinite continuation and act as crosslinking points (noted with c), whereas both end epoxy groups are not crosslinking points (noted with nc).
3. The occurrence of chain-transfer reactions has a net null effect on the final degree of crosslinking because a chain end is not an effective crosslink.
4. The reaction of a secondary hydroxyl group coming from a DGEBA oligomeric species, depicted in Scheme 2(b), does not decrease the degree of crosslinking. This hydroxyl group may turn into a crosslink (c), whereas the subsequent ring opening of the epoxy group leads to another secondary hydroxyl group (nc). The overall effect would be the formation of a crosslinking point per epoxy group reacted, and therefore, DGEBA hydroxyl groups do not have to be considered.
5. The reaction of a primary hydroxyl group from the S2200 results leads eventually to the ring opening of an epoxy group, which does not turn into a crosslinking point (see Scheme 3). As a result, a crosslinking point is lost for each primary hydroxyl group that reacts. However, internal branching points of S2200 can be fully or partially activated into effective crosslinking points in the process.[27] Secondary hydroxyl groups formed by the ring opening of the epoxy would have the same effect as in discussed in point 4. For estimation purposes, we assumed that all of the hydroxyl groups of S2200 could react and that all internal branching points of S2200 could be activated.
6. Having excess anhydride groups does not modify the final degree of crosslinking but results in terminal carboxylic groups instead of hydroxyl groups.

Table III. Thermal Expansion Coefficients below and above the T_g (α_g and α_l, respectively) Obtained by TMA and the ρ_{T0} Values

	DG	DGS2200
α_g (μm m^{-1}·°C^{-1})	56 ± 8	51 ± 6
α_l (μm m^{-1}·°C^{-1})	205 ± 12	210 ± 10
ρ_{T0} (g/cm^3)	1.204 ± 0.001	1.205 ± 0.002

The results are reported as Value ± Error.

7. In the event of tertiary amine regeneration, the reinitiation of a growing chain by the released tertiary amine would account for extra initiator and have the same effect as described in point 2.

We estimated the theoretical υ_e values of the DG and DGS2200 formulations, neglecting the occurrence of regeneration as a first approximation, as follows:

$$\upsilon_e = 3/2 \cdot (n_{\text{epoxy}} + n_{\text{S2200}} - n_{\text{OH,S2200}} - 2n_{\text{initiator}}) \quad (10)$$

where n_{epoxy} and $n_{\text{initiator}}$ are the numbers of epoxy and initiator groups per mass unit, n_{S2200} is the number of branching points in S2200 as represented by the tertiary amide groups, and $n_{\text{OH,S2200}}$ is the number of S2200 hydroxyl groups in the sample. The 3/2 factor arises from the consideration that each crosslink issues three chains and an elastically active network chain is bound to two crosslinks. All of these positive and negative contributions can be derived from the composition in Table I, except the amount of tertiary amide groups. The amount of tertiary amide groups of S2200 was estimated to be 207.6 g/equiv of N, as determined on the basis of the idealized structure shown in Scheme 1, the molar mass of diisopropanolamine and succinic anhydride used for the synthesis of S2200, the loss of water by condensation, and its hydroxyl equivalent of 175 g/mol. Taking into account the composition in Table I, we estimated the υ_e values of the DG and DGS2200 formulations to be 0.00404 and 0.00294 mol/g, respectively. This produced a ratio of 0.73 of DGS2200 with respect to DG. This result was in qualitative agreement with the experimental E'_r determined with DMA.

Assuming that there was some inherent error in the determination of E'_r using DMA and that it was arguable to apply the rubber elasticity theory in the case of thermosets,[22] we attempted to derive υ_e from eq. (4). To do so, we also used eq. (5) and the densities and thermal expansion coefficients in Table III and assumed ideal elastomer behavior as well [$\phi = 1$ in eq. (4)]. For the DG and DGS2200 thermosets, this yielded values of 0.00140 and 0.00078 mol/g, respectively. The experimental υ_e ratio was, therefore, 0.55. There was a remarkable discrepancy between the predicted and experimental υ_e values; this could be ascribed to reasons different than experimental error: (1) topological restrictions leading to an incomplete reaction of epoxy groups, (2) incomplete activation of all of the potential crosslinks from S2200, or (3) the occurrence of regeneration to some extent, which led to more chain ends than expected.

In a previous study,[20] we observed that the occurrence of regeneration during the curing of the DG formulation led to the formation of more carboxylic acid groups than expected.

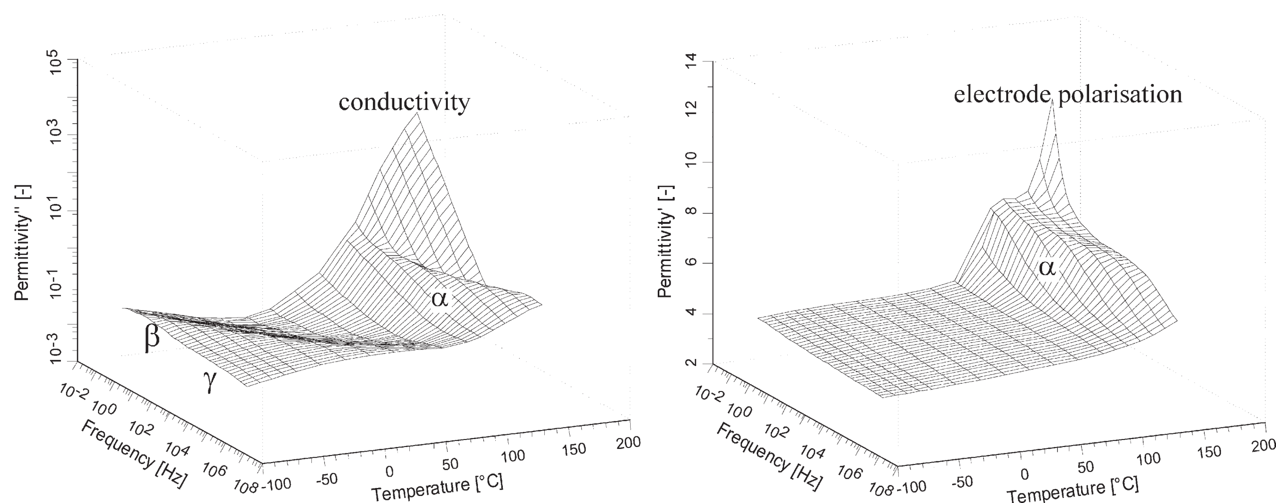

Figure 2. Dependences of the imaginary part [ε'' (left plot)] and real part [ε' (right plot)] of the permittivity versus the frequency and temperature for DG.

Moreover, the overall amount of hydroxyl groups at the end of the process was higher than at the beginning, which could be explained by the occurrence of regeneration. In our previous article, we reported a high conversion at gelation; this was in agreement with the data reported by other authors[25,26] and could be partially explained on the basis of tertiary amine regeneration.[26] However, other authors attributed this to the presence of protic impurities, such as free acid, which may have acted as chain-starting points,[25] or to the occurrence of chain-transfer processes induced by the presence of hydroxyl groups.[28] From the difference between the experimental and predicted υ_e values, we estimated that there was one regeneration event per four reacted epoxy groups. We also observed that the incorporation of S2200 was gradual, so the participation of its hydroxyl groups and the activation of its internal branching points was overestimated; this contributed to the decreases in υ_e of DGS2200 and the ratio between DGS2200 and DG.

Both the predicted and experimental results indicated a significant decrease in υ_e with the incorporation of S2200, but nevertheless, $T_{g\infty}$ of the cured material was not affected accordingly. The incorporation of S2200 into the network structure probably contributed to the decrease in the mobility of the network and, therefore, made up for the decrease in υ_e. Indeed, it was acknowledged that not only υ_e but other factors, such as the rigidity of the polymer backbone, which may reduce the mobility of the network, have an effect on the $T_{g\infty}$ values of cured thermosets.[22,29] We lacked any rigorous demonstration, but we hypothesized that the partial incorporation of S2200 into the network structure may have restricted the mobility of the resulting network because of its hyperbranched structure and the high concentration of crosslinks inside and within the vicinity of S2200 and also to extensive H bonding between the hydroxyl and carbonyl groups within the network structure, similar to other epoxy thermosets modified with hydroxyl-terminated HBPs.[30] One must take into account that (1) an excess of anhydride groups was used in the DGS2200 formulation, (2) both S2200 and anhydride contributed with carbonyl groups, and (3) the overall amount of hydroxyl groups at the end of the process was higher than at the beginning, either as hydroxyl or carboxylic acid groups. The likelihood of H bonding within the network structure increased significantly; this may have contributed to the reduction in mobility of the network and offset the effect of the decrease in the network υ_e; hence, the decrease in $T_{g\infty}$ was limited.

With regard to the thermal expansion of DG and DGS2200 reported in Table III, we observed that the thermal expansion coefficient was almost identical above $T_{g\infty}$, but it was somewhat lower for DGS2200 below $T_{g\infty}$. The values were in good agreement with those reported previously.[17] The decrease in this coefficient in the glassy state, along with the reduction in $T_{g\infty}$, was beneficial because it decreased the generation of internal stresses in the cool-down step after curing and the dimension mismatch to metal substrates.[31] With the experimental error taken into account, the effect was discrete, but this still resulted in a reduction in the formation of microvoids and microcracks and better adhesion to the substrate, which improved the durability of the material. This is of key importance with regard to the use of epoxy–anhydride formulations in electrical applications.[19]

Dielectric Properties

Figure 2 depicts the results of DEA of the DG formulation. From both the imaginary and real parts of ε^*, it was possible to determine the α relaxation of the thermoset associated with the segmental mobility, but analysis of the imaginary part, the loss factor, also allowed us to determine the relaxations more precisely as they appeared as peaks. In the low-temperature range, two secondary relaxation processes, β and γ, were also observed and were connected to local group mobility.

Figure 3 compares the primary α and secondary β and γ relaxations (at 130 and -60°C, respectively) for the DG and DGS2200 formulations. The real part of ε^* increased with decreasing frequency because of the segmental and local relaxation of the network; this led to a higher mobility and, consequently, a higher polarizability. The increase in permittivity was

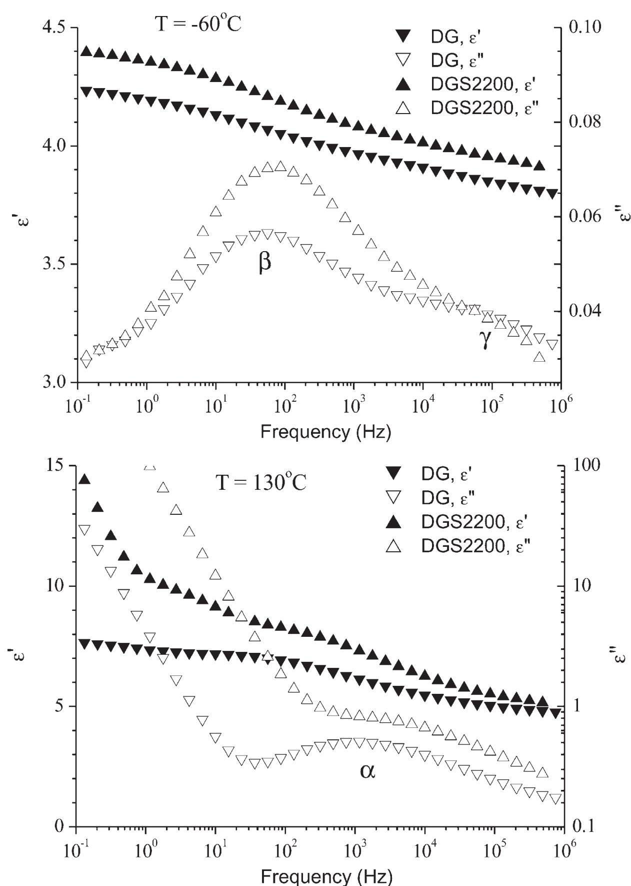

Figure 3. Dependences of the imaginary part (ε'') and real part (ε') of the permittivity versus the frequency at a temperature of −60 and 130°C for DG and DGS2200.

higher in the case of the DGS2200-cured thermoset, as was the intensity of the loss factor peak, in both the α and β relaxations. The fact that the permittivity was higher in DGS2200 than in DG was a positive phenomenon in terms of the specific application, where a high breakdown strength is a key issue. This could have been due to the presence of more polar groups in the network structure, such as the internal ester and amide groups coming from S2200 and the ester and carboxylic acid groups resulting from the reaction of S2200 hydroxyl groups with anhydride. The γ relaxation was not sensitive to the network structure at all because it was most likely associated with the oscillation of small groups or chain ends.

We also appreciated that the α relaxation of DGS2200 occurred at a somewhat higher frequency; this accounted for the higher network mobility and was in agreement with the DMA and calorimetric data (this is more clearly seen in the relaxation map in Figure 4, which is discussed later). Once the material was relaxed, the increase in permittivity was much higher after the α relaxation of the network than in the other relaxations. The higher concentration of polar groups in the DGS2200 formulation, coupled with its looser network structure in the relaxed state, resulted in a significant enhancement in the polarizability of the material and, consequently, a significant increase in the permittivity, especially at the longest observation times.

Network Relaxation Dynamics

The dynamics of the α relaxation of the DG and DGS2200 cured materials were studied by TTS of DMA and dielectric data. First, we checked the feasibility of the TTS adjustment using DMA data and the data analysis software provided by TA Instruments. A good adjustment was obtained with the E'' curve, with the reference temperature taken as the one with a centered local maximum with respect to the frequency, from T_{ref} to $T_{ref} + 50$. However, given that the experimental frequency range of the DMA data was somewhat narrow (from 0.1 to 20 Hz), we attempted to analyze both the dynamic mechanical and dielectric data at the same time to extend the frequency range and to obtain a more reliable adjustment. We determined the τ values of all of the dielectric relaxations at different temperatures and plotted them in a relaxation map in Figure 4. The τ values of the DMA data corresponding to the α relaxation were determined with the loss modulus (E'') data and plotted them in the same figure. Some relevant facts need to be highlighted:

1. DG and DGS2200 showed very similar relaxation behaviors; this was in agreement with the DMA data.
2. The α relaxation of DGS2200 occurred at a somewhat lower temperature than that of DG and accounted for a higher network mobility, as explained previously.
3. There was an excellent superposition between the τ values obtained by both techniques. That is, the τs determined with DMA and DEA were comparable. Indeed, there was a frequency range in which results obtained by both techniques overlapped. In general, good agreement between the τ values obtained with different techniques has been reported.[32,33] Ramis et al.[33] reported that the mechanical τ was longer than that of the dielectric relaxation. In that case, however, they determined the mechanical τ from the maximum in tan δ, which increased τ (or decreases the frequency). In this case, both the DEA and DMA τ values were derived from the loss dielectric factor (ε'') and the mechanical loss factor (E''), and this led to more consistent results.

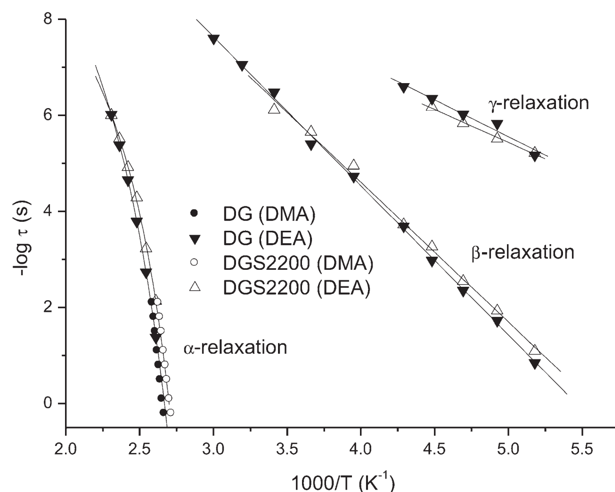

Figure 4. Relaxation map of DG and DGS2200 determined by DMA and DEA, respectively.

Journal of Applied Polymer Science

Table IV. Summary of the TTS of the Dielectric Data with the WLF Equation

	DG	DGS2200
T_{ref} (°C)	109	101
C_1	9.93 ± 0.54	10.11 ± 0.48
C_2 (°C)	55.9 ± 4.5	58.1 ± 4. 5
E_A (kJ/mol)	497 ± 49	466 ± 42
f_g	0.0437 ± 0.0024	0.0429 ± 0.0020

The results are reported as Value ± Error.

Although it is normal to also use other expressions for the analysis of dielectric relaxations. such as the Vogel–Taman–Fulcher[33] or the Kolrausch–Williams–Watt[34] equations, we fitted the experimental τ of the α relaxation of combined the DEA and DMA data to the WLF equation and interpreted the results in terms of free volume.[23] The results of this adjustment are reported in Table IV. Note that we used the calorimetric $T_{g\infty}$ as a reference temperature for the adjustment. As suggested by the relaxation map, the relaxation in both materials was very similar; this was confirmed by the similar C_1 and C_2 adjustment parameters. Both E_A and f_g were within the order of magnitude for thermosets.[22] It is worth noting that despite the significant decrease in crosslinking density with the incorporation of S2200, as reported in Figure 1 and Table II, f_g at T_g, which was associated with the mobility of the network at the relaxation, was hardly affected. This was in agreement with the only slightly lower $T_{g\infty}$ of DGS2200 in comparison with that of DG. The fact that $T_{g\infty}$ and the relaxation of the network appeared to be connected to the free-volume behavior[23] or mobility[22,29] rather than υ_e was not always evident because, in thermosets, T_g is often associated with the degree of crosslinking during a curing process,[22,35,36] but this, in turn, is related to the available free volume, which obviously decreases as the crosslinking proceeds and reduces the mobility of the growing network. The incorporation of S2200 may have led to a looser network structure in terms of the overall crosslinking density but, at the same time, one with a restrained mobility and lower free volume before the relaxation because of the existence of numerous H-bonding interactions.

Table V reports the results of the adjustment of τ of the secondary β and γ relaxations with an Arrhenius law, such as that in eq. (6), and no differences were observed between them. This indicated that the introduction of S2200 into the network structure did not alter the nature of the local mobility dynamics either.

Table V. E_A Values of the Secondary Relaxations Obtained by DEA

	E_A (kJ/mol)	
	γ relaxation	β relaxation
DG	29 ± 3	59 ± 1
DGS2200	26 ± 2	56 ± 2

The results are reported as Value ± Error.

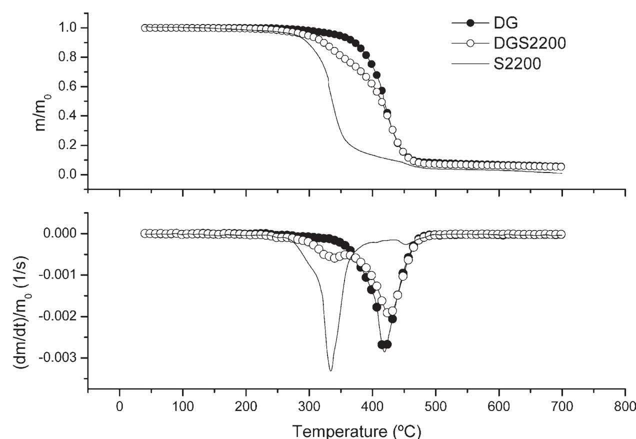

Figure 5. Degradation curves at 10°C/min in a nitrogen atmosphere of the cured materials and S2200 (m/m_0 is the normalized mass of the sample, where m is the mass at any stage of the process and m_0 is the mass at the beginning. $(dm/dt)/m_0$ is the normalized rate of mass loss).

Thermal Degradation

Figure 5 and Table VI summarize the results of the thermal degradation of the cured materials at 10°C/min. We observed that the thermal stability decreased significantly with the addition of S2200, in terms of the temperatures at 2 and 5% mass loss ($T_{2\%}$ and $T_{5\%}$, respectively), whereas the main peak temperature remained unaltered. These results were in agreement with a previous study that used an analogous hyperbranched poly(ester amide).[17] From the shape of the degradation curves in Figure 5, we observed that the degradation of DGS2200 took place in two distinct processes, with the former taking place within the temperature range of the degradation of neat S2200 and the latter taking place within the decomposition range of the unmodified DG formulation. One might think that the lower overall crosslinking density of DGS2200 explained this early decomposition, but one must bear in mind that the secondary ester groups of S2200 were less thermally stable than the primary ester groups formed by the epoxy–anhydride copolymerization. Moreover, secondary ester groups were also formed by the reaction of the secondary hydroxyl groups present in the oligomeric DGEBA and after the reaction of the S2200 hydroxyl groups. We estimated that a mass loss of about 28% was associated with the first process; this was higher than the amount of S2200 and excess anhydride in the mixture. Therefore, part of the epoxy–anhydride copolymer was able to decompose in the first process as a consequence of the effective incorporation of S2200 into the network structure. The rest of the material would have had a thermal stability similar to that of the unmodified DG

Table VI. Summary of the Thermal Degradation of the Cured Materials at 10°C/min in a Nitrogen Atmosphere

	$T_{2\%}$ (°C)	$T_{5\%}$ (°C)	Peak temperature (°C)	Char at 700°C (%)
DG	317 ± 1	352 ± 1	423 ± 1	6.32 ± 0.82
DGS2200	260 ± 12	298 ± 8	427 ± 2	5.94 ± 0.52

The results are reported as Value ± Error.

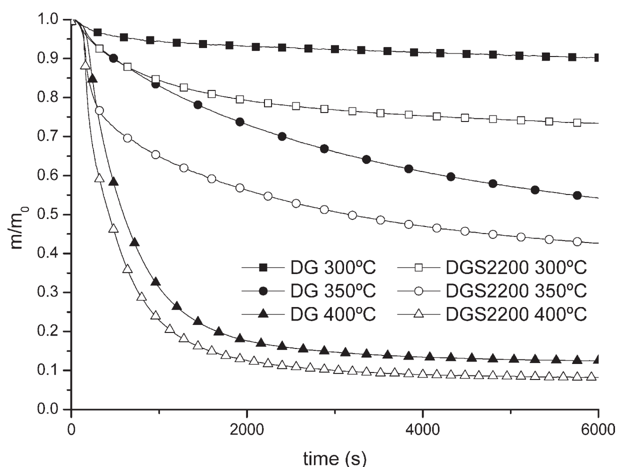

Figure 6. Isothermal degradation of the cured materials at different temperatures in a nitrogen atmosphere (m/m_0 is the normalized mass of the sample, where m is the mass at any stage of the process and m_0 is the mass at the beginning).

formulation, with primary ester groups that were less degradable than the secondary ester groups; hence, the peak temperatures were similar.

The isothermal degradation of the two formulations was studied. Figure 6 shows how the thermal degradation of the DGS2200 formulation was much faster than that of DG. The DGS2200 formulation started to decompose significantly before the isothermal temperature was achieved (up to 30% at 400°C), despite the high heating rate, in comparison with DG (up to 10% at 400°C). To further clarify the degradation mechanism of the DGS2200 and DG formulations, the mass fraction of DGS2200 was corrected by its division by the fraction of unmodified epoxy–anhydride, and it was plotted against the mass of the degradation of unmodified DG formulation. In Figure 7, it is clearly shown that once the degradation of the S2200 structure took place, the degradation rate of the remaining material was the same as that of the unmodified DG. This result was in good agreement with the overlapping of the degradation peaks shown in Figure 5.

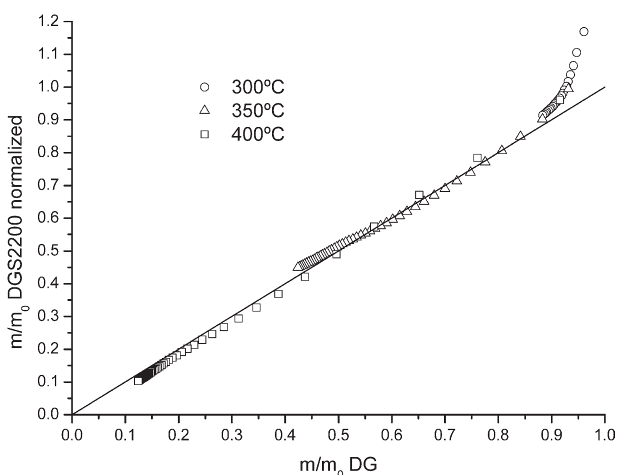

Figure 7. Corrected weight loss of DGS2200 against DG corresponding to the isothermal degradation experiments (m/m_0 is the normalized mass of the sample, where m is the mass at any stage of the process and m_0 is the mass at the beginning).

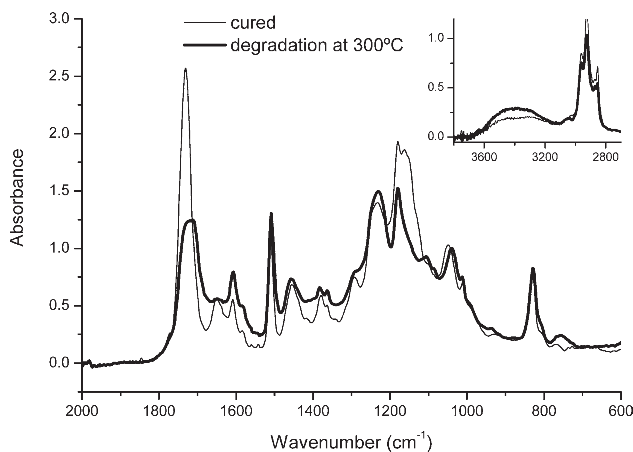

Figure 8. FTIR spectra of the cured DGS2200 formulation before and after degradation at 300°C.

The materials were analyzed after the isothermal treatment. At 400°C, only a small amount of char was left. However, when the treatment was performed at 300°C, a material with a similar appearance to that of the cured one was obtained, with a T_g of 108 and 97°C for the DG and DGS2200 formulations, respectively. Figure 8 compares the spectra corresponding to the DGS2200 thermoset after curing and after degradation at 300°C (there was a 27% weight loss after this treatment). We observed a significant reduction in the intensity of the ester band at 1730 cm^{-1}, a shift of the band associated with carboxylic acid down to 1700 cm^{-1}, a decrease in the tertiary amide band at 1650 cm^{-1}, and a growth in the O—H stretching band between 3200 and 3600 cm^{-1}. These observations were in agreement with the occurrence of a β-elimination mechanism, which led to carboxylic acid and C=C formation, as reported previously,[2,4,6] and also indicated the early decomposition of the S2200 fraction.

To sum up, S2200 had a positive effect on the degradation rate of DGS2200, especially at the beginning; this resulted in a shorter degradation time and may have helped to optimize the thermal pyrolysis of the coating and its removal from the substrate.

Thermal Conductivity

In the case of polymers, phonons are the primary mechanism of heat conduction. The thermal conductivity of polymers depends on many factors, namely, the chemical constituents, structure type, molecular density distribution, bond strength, and type of defects or structural faults. Also, the size of intermediate range order, processing conditions, and temperature play significant roles in the heat-transfer phenomenon.[37] Additionally, the incorporation of each new phase into the investigated system leads to the enhancement of phonon scattering at the interface.[38]

Table VII. Thermal Conductivities of DG and DGS2200 at 300 K

	Thermal conductivity ($W \cdot m^{-1} \cdot K^{-1}$)
DG	0.187 ± 0.009
DGS2200	0.162 ± 0.008

The results are reported as Value ± Error.

The results of the thermal conductivity measurements at 300 K for each sample are shown in Table VII. One can see that for the modified DGS2200 samples, the thermal conductivity decreased in comparison with the reference DG sample. The addition of the hyperbranched polyesteramide S2200 possibly increased phonon scattering, and as a result, heat transfer within the sample was hindered. This was not beneficial from the application point of view because effective heat dissipation is of key importance for preventing excessive temperatures during the operation of an apparatus.[39] However, the values were still valid and within specifications when we took into the fact that a mineral filler is, nevertheless, used to improve the thermal conductivity, among other reasons. There was an important difference between DG and DGS2200 in terms of network υ_e, and this might have contributed to the reduction in the thermal conductivity, but the available free volume in the network was very similar in both cases, as indicated by the calculations based on the TTS analysis and the similar $T_{g\infty}$ values.

Mechanical Tests

The results of the mechanical tests are shown in Table VIII. We observed that the use of S2200 increased both IS, as in previous works,[17] and also the microhardness. The increase in IS could be justified by the lower υ_e of the DGS2200 network and its better damping capability compared with DG, as observed in the DMA of these formulations. This effect was discrete, however, compared with other thermosetting formulations modified with phase-separating HBPs.[9]

The use of S2200 was, nevertheless, beneficial because it improved the resistance of the thermoset to demanding mechanical conditions, such as abrasion and crack resistance, where toughness plays a significant role.[19] Another important factor is the thermal coefficient difference between the matrix and the filler. The fact that the thermal expansion coefficient of DGSS2200 below $T_{g\infty}$ was lower (see previous discussion), coupled with its enhanced toughness, may have both contributed to the increase in the durability of the filler-reinforced material.[19]

CONCLUSIONS

The use of S2200 as a polymeric modifier of epoxy–anhydride thermosets for electrical applications was explored. The effect of S2200 on relevant properties was assessed and related to the network structure of the modified thermoset.

The incorporation of S2200 significantly reduced the crosslinking of the resulting epoxy–anhydride thermosets. However, $T_{g\infty}$ was hardly affected and was still within the application specifications. This was ascribed to a mobility restriction imposed by the incorporation of S2200 into the network structure and

Table VIII. Summary of the Mechanical Tests Performed on the DG and DGS2200 Samples

	IS (kJ/m^2)	HKN
DG	3.0 ± 0.4	12.7 ± 1.0
DGS2200	3.5 ± 0.6	18.1 ± 1.2

The results are reported as Value ± Error.

extensive H bonding within the network structure; this offset the increase in the free volume caused by the reduction in υ_e. DEA showed that the permittivity increased with the incorporation of S2200; this could be explained by the significant increase in the amount of polar groups within the network structure and the lower υ_e of the resulting thermoset. This was beneficial from the application point of view because of the higher breakdown strength of the modified thermoset. Both DMA and DEA gave a consistent picture of the network structure of the analyzed thermosets, which had very similar network relaxation dynamics. The fact that the thermal conductivity was reduced by the incorporation of S2200 was not beneficial because it made difficult the dissipation of heat, but when we took into account the fact that inorganic fillers are used for that purpose, this effect was of little significance. The lower thermal expansion coefficient of the modified thermoset reduced the thermal expansion mismatch between the matrix and the filler and, thus, reduced the formation of internal stresses. This, coupled with the enhanced IS, should contribute significantly to enhance the durability of the material.

S2200 decreased the thermal stability of the formulation and, thus, shortened the degradation time. This effect was observed primarily at the beginning of degradation and could be associated with the thermal decomposition of S2200 and the fraction of epoxy–anhydride copolymer directly attached to S2200. This opened the way for the optimization and control of the thermal degradation of the components once their service lives are over to recover the substrate.

To sum up, S2200 is a promising polymeric modifier for use in the modification of epoxy–anhydride formulations because the thermal degradability of the modified thermosets is significantly enhanced and its relevant material properties are not sacrificed; this fulfills the demands of application.

ACKNOWLEDGMENTS

The authors thank Ministerio de Ciencia e Innovación (MICINN), Fondo Europeo de Desarrollo Regional (FEDER), and Generalitat de Catalunya (contract grant numbers MAT2011-27039-C03-01, MAT2011-27039-C03-02, JCI-2010-06187, and 2009-SGR-1512) for financial support. DSM is also acknowledged for their kind provision of the materials for this study.

REFERENCES

1. Chen, J. S.; Ober, C. K.; Poliks, M. D. American Chemical Society, Polymer Preprints, Division of Polymer Chemistry, vol. 41. Published by American Chemical Society, Washington, DC, USA, **2000**; p 1842.

2. Chen, J. S.; Ober, C. K.; Poliks, M. D. *Polymer* **2002**, *43*, 131.
3. Chen, J.-S.; Ober, C. K.; Poliks, M. D.; Zhang, Y.; Wiesner, U.; Cohen, C. *Polymer* **2004**, *45*, 1939.
4. Gonzalez, L.; Ramis, X.; Salla, J. M.; Mantecon, A.; Serra, A. *Polym. Degrad. Stab.* **2007**, *92*, 596.
5. Arasa, M.; Ramis, X.; Salla, J. M.; Mantecon, A.; Serra, A. *Polym. Degrad. Stab.* **2007**, *92*, 2214.
6. Gimenez, R.; Fernandez-Francos, X.; Salla, J. M.; Serra, A.; Mantecon, A.; Ramis, X. *Polymer* **2005**, *46*, 10637.
7. Cervellera, R.; Ramis, X.; Salla, J. M.; Mantecon, A.; Serra, A. *J. Polym. Sci. Part A: Polym. Chem.* **2006**, *44*, 2873.
8. Voit, B. *J. Polym. Sci. Part A: Polym. Chem.* **2000**, *38*, 2505.
9. Boogh, L.; Pettersson, B.; Manson, J.-A. E. *Polymer* **1999**, *40*, 2249.
10. Mezzenga, R.; Manson, J. A. E. *J. Mater. Sci.* **2001**, *36*, 4883.
11. Ratna, D.; Simon, G. P. *Polymer* **2001**, *42*, 8833.
12. Ratna, D.; Varley, R.; Simon, G. P. *J. Appl. Polym. Sci.* **2003**, *89*, 2339.
13. Xu, J.; Wu, H.; Mills, O. P.; Heiden, P. A. *J. Appl. Polym. Sci.* **1999**, *72*, 1065.
14. Blanco, I.; Cicala, G.; Lo Faro, C.; Motta, O.; Recca, G. *Polym. Eng. Sci.* **2006**, *46*, 1502.
15. Mezzenga, R.; Plummer, C. J. G.; Boogh, L.; Manson, J. A. E. *Polymer* **2001**, *42*, 305.
16. Sangermano, M.; Malucelli, G.; Bongiovanni, R.; Priola, A.; Harden, A. *Polym. Int.* **2005**, *54*, 917.
17. Morell, M.; Ramis, X.; Ferrando, F.; Yu, Y.; Serra, A. *Polymer* **2009**, *50*, 5374.
18. Foix, D.; Erber, M.; Voit, B.; Lederer, A.; Ramis, X.; Mantecon, A.; Serra, A. *Polym. Degrad. Stab.* **2010**, *95*, 445.
19. Valette, L.; Jiang, L. Y.; Ji, D.; Karunakaran, K. Electrical Insulation Conference, EIC **2011**, Annapolis, MD, IEEE Computer Society, Washington, DC, 2011; p 459.
20. Fernández-Francos, X.; Rybak, A.; Sekula, R.; Ramis, X.; Serra, À. *Polym. Int.* [Online early access]. DOI: 10.1002/pi.4259. Published Online: May 16, **2012**. http://onlinelibrary.wiley.com/doi/10.1002/pi.4259/full. Accessed on May 16, 2012.
21. Foix, D.; Yu, Y.; Serra, A.; Ramis, X.; Salla, J. M. *Eur. Polym. J.* **2009**, *45*, 1454.
22. Pascault, J. P.; Sautereau, H.; Verdu, J.; Williams, R. J. J. Thermosetting Polymers; Marcel Dekker: New York, **2002**.
23. Ferry, J. D. Viscoelastic Properties of Polymers; Wiley: New York, **1980**.
24. Miyagawa, H.; Mohanty, A. K.; Misra, M.; Drzal, L. T. *Macromol. Mater. Eng.* **2004**, *289*, 629.
25. Dusek, K.; Lunak, S.; Matejka, L. *Polym. Bull. (Berlin)* **1982**, *7*, 145.
26. Mauri, A. N.; Galego, N.; Riccardi, C. C.; Williams, R. J. *J. Macromolecules* **1997**, *30*, 1616.
27. Dusek, K.; Duskova-Smrckova, M. *Macromolecules* **2003**, *36*, 2915.
28. Fernandez-Francos, X.; Cook, W. D.; Salla, J. M.; Serra, A.; Ramis, X. *Polym. Int.* **2009**, *58*, 1401.
29. Sue, H. J.; Puckett, P. M.; Bertram, J. L.; Walker, L. L. *Am. Chem. Soc. Symp. Ser.* **2000**, *759*, 171.
30. Ratna, D.; Simon, G. P. *Polym. Eng. Sci.* **2001**, *41*, **1815**.
31. Lange, J.; Toll, S.; Manson, J. A. E.; Hult, A. *Polymer* **1995**, *36*, 3135.
32. Montserrat, S.; Roman, F.; Colomer, P. *Polymer* **2003**, *44*, 101.
33. Ramis, X.; Calventus, Y.; Cadenato, A.; Roman, F.; Morancho, J. M.; Colomer, P.; Salla, J. M.; Montserrat, S. *Prog. Org. Coat.* **2004**, *51*, 139.
34. Beiner, M.; Ngai, K. L. *Macromolecules* **2005**, *38*, 7033.
35. Pascault, J. P.; Williams, R. J. J. *J. Polym. Sci. Part B: Polym. Phys.* **1990**, *28*, 85.
36. Ramis, X.; Salla, J. M. *J. Polym. Sci. Part B: Polym. Phys.* **1997**, *35*, 371.
37. Han, Z.; Fina, A. *Prog. Polym. Sci. (Oxford)* **2011**, *36*, 914.
38. Felba, J. In Nano-Bio-Electronic, Photonic and MEMS Packaging; Wong, C. P., Moon, K.-S., Li, Y., Eds.; Springer: New York, **2010**.
39. Filippakou, M. P.; Karagiannopoulos, C. G.; Agoris, D. P.; Bourkas, P. D. *Electr. Power Syst. Res.* **2001**, *57*, 141.